EVALUATION AND MODULATION OF ELECTROSPUN COLLAGEN NANOFIBER DIAMETER

By

Heleine Vanessa Ramos Avilez

A project submitted in partial fulfillment of the requirements for the

MASTER OF ENGINEERING DEGREE
In
CHEMICAL ENGINEERING

UNIVERSITY OF PUERTO RICO
MAYAGÜEZ CAMPUS
2016

Approved by:

_____   _____
Jorge Almodóvar Montanez, Ph.D   Date
President, Graduate Committee

_____   _____
Madeline Torres Lugo, Ph.D   Date
Member, Graduate Committee

_____   _____
Magda Latorre Esteves, Ph.D   Date
Member, Graduate Committee

_____   _____
Silvina Cancelos, Ph.D   Date
Representative of Graduate Studies

_____   _____
Aldo Acevedo Rullan, Ph.D   Date
Chairperson of the Department

ABSTRACT

Electrospinning is a process for generating ultrathin fibers from a polymeric fluid using an electric field. It is relatively easy to implement, but it is itself complex due to the many parameters that govern the formation of the fibers. In this project, nanofibers from collagen dissolved in acetic acid were produced. The effect of flow rate (Q) and voltage (V) on diameter fiber (D) was evaluated, and a prediction model of the fiber diameter was identified. Also, an expression for the fiber diameter as a function of flow rate was found. Results reveal that fibers obtained had a uniform morphology with no beads-like defects. The flow rate significantly effects the fiber diameter. There is an almost linear increase on the average fiber diameter with the increase of the flow rate. The voltage has low influence over fiber diameter, at the process conditions to which experimental trials were carried out. The identified model predicts the fiber diameter with an average error of 16.75% and, fiber diameter varies proportionally to $Q^{1/6}$.

RESUMEN

El electrohilado es un proceso que usa un campo eléctrico para producir fibras ultrafinas de un fluido polimérico. Es fácil de implementar, pero de naturaleza compleja por los múltiples parámetros que influyen en la formación de las fibras. En este proyecto se generaron fibras de colágeno disuelto en ácido acético usando electrohilado, se evaluó el efecto del voltaje y la velocidad de flujo en el diámetro de las fibras obtenidas y se identificó una expresión para el diámetro de fibra en función de dichas variables. Las fibras resultantes fueron uniformes, sin defectos en forma de abalorios ovalados. La velocidad de flujo tiene una influencia sobre el diámetro estadísticamente significativa. Además existe un incremento casi lineal del diámetro con el incremento de la velocidad de flujo. Mientras que el voltaje tiene menor influencia sobre el diámetro de fibra a las condiciones experimentales trabajadas. El modelo identificado en la literatura predice el diámetro de fibra con un error de 16.75% y los datos experimentales varían proporcionalmente a la velocidad de flujo elevada a un 1/6.

DEDICATION

I dedicate this project to Jesus Christ, for his grace and his love, to my loving husband Jorge and to my little daughter Carol.

ACKNOWLEDGEMENTS

TABLE OF CONTENTS

TABLE OF FIGURES

INTRODUCTION

Electrospinning is an efficient technique used to manufacture nanoscale fibrous structures[1,2]. In this process, electrostatic forces are used to obtain fine fibers from a droplet of polymer solution, which is deposited onto a grounded collector[3]. Electrospun polymeric nanofiber has been produced for applications in different fields including tissue engineering[4–9], filtration[10–13], catalysis[14,15] and biosensors[16–19]. Its broad applicability is due to the simplicity of the method. Fiber properties such as small fiber diameter, high porosity, tunable orientation and surface area as well as a range of synthetic and natural polymers[20–22] as collagen[23–26], which has been used in a variety of tissue engineering applications [25,27,28]. Fibers from biological materials are preferred due to better clinical functionality[29], specifically fibers from collagen are used because of their biocompatible and biodegradable properties[30] and it is also the main protein in mammals[27]. At present, electrospinning is the most widely adopted method for producing collagen fibers. In general, volatile fluoroalcohols such as 1,1,1,3,3,3-hexafluoro-2-propanol (HFP) or 2,2,2-trifluoroethanol (TFE) solvents are used [29]. However, the toxic nature of these chemicals may impede the biochemical cross-talk between the tissue and the engineered spun material adversely affecting cells[30], thus, it limits their application in regenerative medicine and tissue engineering. It has been shown that HFP transforms collagen to gelatin. Additionally, using either HFP or TFE in electrospinning of collagen yields collagen nanofibers that do not swell in aqueous media like other collagenous structures, but instead are readily soluble in water, tissue fluids or blood [29].

Nanofibers from collagen dissolved in a benign solvent, produced via electrospinning were achieved in our laboratory[31]. We observed a strong correlation between fiber diameter and process parameters in preliminary experiments; however, we obtained unpredictable fiber diameters. Also, the literature shows an unclear relation between those parameters and fiber diameter[32,33]. Thus, we decided to evaluate the effect of flow rate and the voltage on fiber diameter. Although, there are multiple parameters involved in the process of electrospinning we choose these variables since they are parameters that can be easily manipulated in the lab to obtain a determined fiber size. It is important to control fiber diameter because it is strongly correlated with mechanical properties of the scaffold and it determines cell morphology, phenotype, and differentiation[34]. Also, we used a prediction model of the fiber diameter scaled for the diameter of the jet far from the nozzle. Feng (2002)[35] obtained the governing equations for the steady jet region of electrospinning. From these equations Gadkari (2014),[36] proposed a scaling and obtained an expression for the radius of the jet. We employed that expression to predetermine the electrospun fiber diameter using the polymer solution flow rate and the applied voltage. The results from this project will be useful for better control of the electrospinning process in future research and applications.

1. BACKGROUND

1.1. Electrospinning

Electrospinning is a method that uses an electric field to fabricate nonwoven fibrous polymer mats on the nanoscale[1,3,26], as shown in Figure 1. Electrospinning is an old technique known more than a century ago[37]. In 1902, Cooley and Morton individually patented methods and devices for electrically dispersing fluids[37]. In
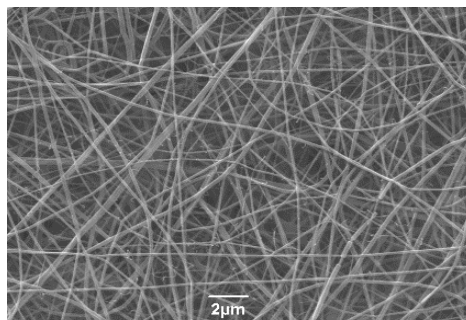
Figure 1. SEM image of nanofibers produced by electrospinning

1934, Formhals patented a process and an apparatus for the production of artificial filaments, which used electric charges[38]. With these devices, he produced fibers of cellulose acetate in acetone/alcohol solution as the solvent. Later on, Formhals published other works in which he improved some issues and disadvantages of the first publication [39,40]. He increased the needle tip to collector distance, this change improved the fiber morphology. After that, he described the use of multiple nozzles for the simultaneous spinning of a number of fibers from the same polymer solution as well as a means to direct the fiber jets toward the collector. In 1940, Formhals patented a new process in which a polymer solution was directly electrospun onto a moving base thread to generate composite fibers [41]. In the early 1960s Taylor published in a series of papers[42,43] focused in a better understanding of the electrospinning process, he investigated how the polymer droplet at the end of a nozzle behaves when an electric field was applied [43]. He studied how the droplet developed into a

cone (Taylor cone) when the surface tension was balanced by electrostatic forces[41]. Since then a lot of work has been published [7,44–47] and nowadays, electrospinning has gained widespread interest as a technique for production of nanofibers for applications in tissue engineering and others wide variety of fields.

The fibers produced via electrospinning have diameters in the range of 50-1000 nm, high porosity and nearly double the surface area of thin films[20]. In general, the surface topography, fiber morphology, diameter, and orientation are governed by solution properties and operating conditions[48]. These fibrous structures have great applications such as wound dressings[49,50], drug delivery materials[3,51,52] and tissue-engineering[53,54]. As scaffold, they have the advantages that can be manufactured from biodegradable and biocompatible polymers and in scale similar to the extracellular matrix (ECM) of native tissues. These scaffolds act as a support to cells[1].

Electrospinning apparatus is composed of a high voltage power supply, a syringe with a nozzle and a syringe pump, and a metal collector[37,55]. Figure 2 displays a schematic diagram of the apparatus. The process consists in cone Taylor formation, jet initiation, elongation of the jet, the whipping of the jet and solidification of the jet on collector[1].
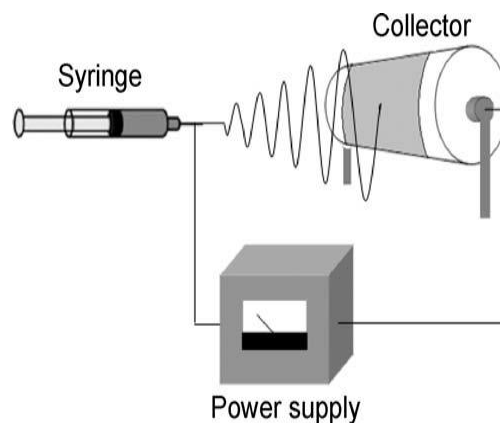
Figure 2. Electrospinning apparatus from[87]

The polymer solution is supplied to the system using the nozzle of the syringe and it is pulsed by the pump. Initially, a drop of polymer solution remains at the tip of the needle due to surface tension. Then, a high-voltage power between the nozzle and the collector is applied. As this electrical voltage intensifies the polymer solution at the needle tip elongates to form a conical shape known as the Taylor cone[3,20,37]. At a critical voltage, the electrical forces overcome the surface tension of the polymer solution, at this point, a polymer jet is ejected from the tip of the Taylor cone and is directed to the target or collector [30,37]. Before reaching the collector, the jet is subject to a series of forces such as electrostatic force, drag force, gravity, columbic repulsion force, surface tension and viscoelastic forces electrically driving bending instabilities. On its way, the solvent evaporates, and the jet gradually thins and elongates in the air forming fibers [3,26,37,55]. These fibers can be deposited on a stationary collector or rotating drum[37].

1.2. Processing parameters in electrospinning

Electrospinning is deceptively simple, but the process itself is indeed complicated because many parameters influence the characteristics of the obtained fibers. These parameters can be combined into the following groups: solution parameters, processing parameters, and ambient parameters. Table 1 shows details. The influence of most of the parameters on fiber diameter is not clear yet, and it is hard to make definitive comparisons with experimental data because each parameter is strongly coupled to other parameters and operating conditions. Now, the results of various researches which studied influence of the parameters of electrospinning on the morphology and fiber diameter are presented.

Table 1. Processing parameters in the electrospinning in electrospinning

Electrospinning Parameters	
Solution properties	Viscosity
	Polymer concentration
	Electrical conductivity
	Surface tension
Processing conditions	Applied voltage
	Flow rate
	Distance from needle to collector
Ambient conditions	Temperature
	Humidity

1.2.1. **Solution properties**

1.2.1.1. **Concentration and Viscosity**

Zong et al., (2002)[56] investigated the structure and morphology of electrospun membranes from poly(D, L-lactic acid) (PDLA) in dimethyl formamide. They found that there was a directly proportional relationship between the polymer concentration and the solution viscosity. Also, these variables determine the fiber morphology. Figure 3 displays changes in the fiber morphology from the full beads structure (lower concentration and viscosity) to the uniform fiber and without beads (higher concentration and viscosity). At concentrations below 20 wt%, they could not obtain fibers neither at concentrations higher than 40 wt% due to the high viscosity of the solution that hindered the electrospinning process[56]. At lower concentrations, the fibers are not completely dried before reaching the target, indicating that the electric field applied is unable to stretch the jet. Therefore, the fibers fall onto the collector without sufficient stretching[56]. But when the solution viscosity is low there is a better yield of electrospinning process and a higher stretching rate because the stretching is opposed to viscous forces. Also, low viscosities produce thinner fibres[49].
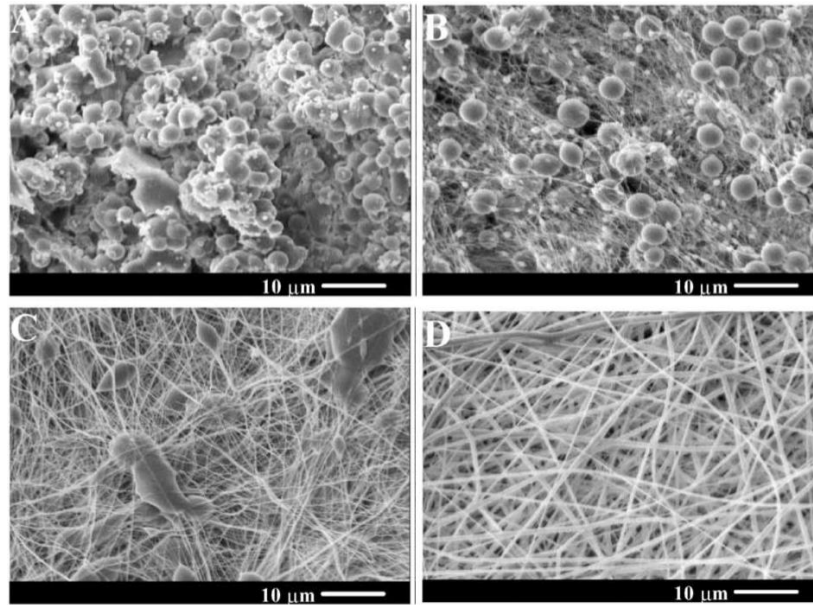
Figure 3. Concentration effect on microstructures of electrospun PDLA nanofibers at voltage of 20 kV, feeding rate of 20 ml/min, and concentration of (A) 20 wt%; (B) 25 wt%; (C) 30 wt% and (D) 35 wt%, from [56].

1.2.1.2. Electrical conductivity

Electric conductivity is directly related with the charge density (I/Q) [21] of a jet. Where *I* is the electrical current and Q is the flow rate. If the rest of parameters are kept constant and the conductivity is increased then, the jet is more elongated by the applied electric field [3,58]. Therefore, fibers with smaller diameter are obtained. However that is not always the case, Rutledge et al., (2001) [59] investigated the influence of conductivity on fiber diameter from polycaprolactone (PLC) solutions. They found that when the conductivity is higher, the fiber diameter is reduced after showing a minimum. Due their results (Figure 4), they think that the relation between conductivity and fiber diameter is more complex[59]. Results obtained by Angammana and Jayaram, (2008)[60] concluded a similar behavior (Figure 5). They observed that the fiber diameter decreases with

increasing solution conductivity, it achieves a minimum value and following it increases

again with increasing solution conductivity[60].
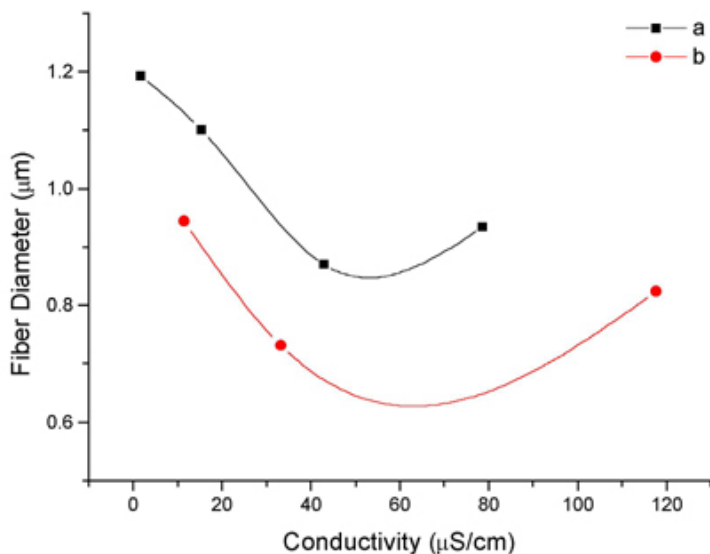
Figure 4. Average fiber diameter versus conductivity. (a) in black, 10% PCL in 3:1 toluene:methanol (b) in red, 15% PCL in 3:1 toluene:methanol, from [59].
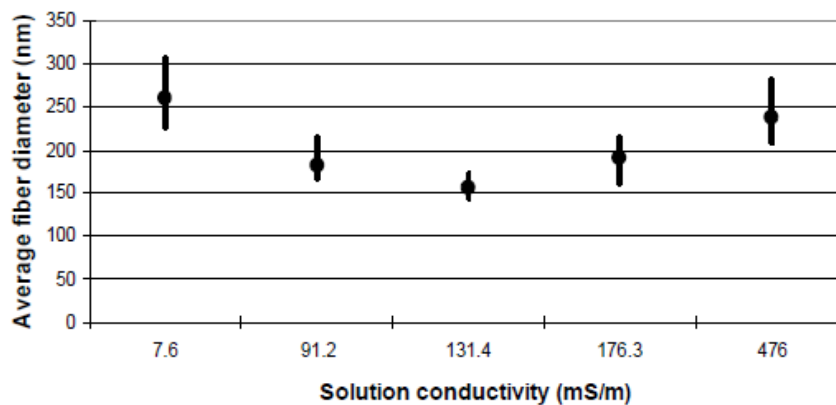
Figure 5. Average fiber diameter vs. solution conductivity at electrode gap distance of 210 mm and applied voltage of 15 kV, from [60].

The conductivity can be modified using additives for improving the production rate of

electrospinning and remove defects such as beads. The formation of beaded fibers is

frequently observed in electrospinning. Fong et al., (1999) [61] showed that it is possible to produce fibers without beads by increasing of the conductivity of the polymer solution (Figure 6Figure 6). They used NaCl for increasing the conductivity and hence net charge density of poly(ethylene oxide) (PEO) solution in water. Hang et al., (2006) achieved a high solution conductivity by using formic acid with a small amount of pyridine to dissolve nylon and obtained ultrathin (3 nm) electrospun nylon fibers and without beads [62].
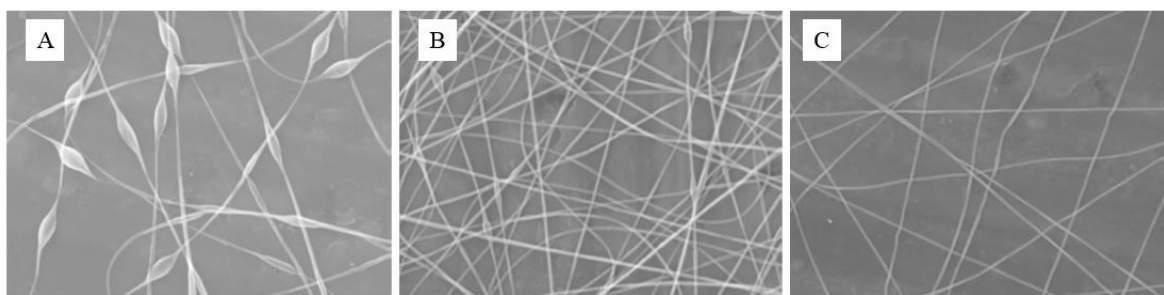
Figure 6. Variation of beaded fibers as net charge density changes due to the addition of NaCl. The electric field is 0.7 kV/cm. The weight fraction of PEO is 3.0%. A. I/Q=1.23C/L. B. I/Q= 6.57C/L.C I/Q= 28.8C/L, from [62].

1.2.1.3.   Surface tension

Surface tension determines the drop size of the polymer solution at the exit of the capillary. A small surface tension is convenient due a smaller threshold voltage is needed to overcome it [63]. It improves process efficiency, has a significant effect on the diameter and morphology of fiber[64]. Wang, He and Xu (2008) added surfactant TritonR X-100 to a poly(vinyl pyrrolidone) polymer solution, whereby achieved a considerable reduction in surface tension as shown in Figure 7A. Consequently, the fiber diameter markedly decreased too (Figure 7B). Moreover, both the electrospinability and the morphology of electrospun nanofibers were enhanced[63].
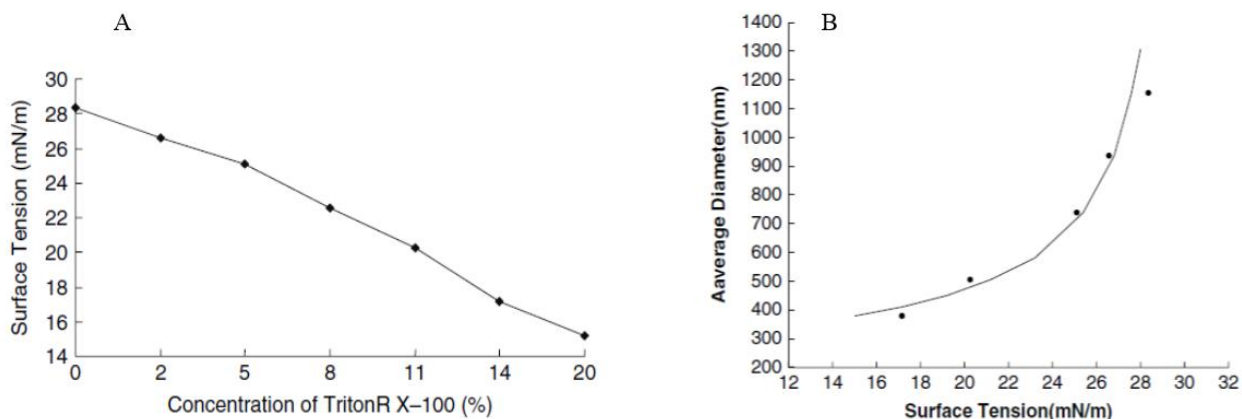
Figure 7. A. Surface tension of 35 wt% PVP solution with different TritonR X-100 concentrations. B. Effect of the surface tension on the diameter of the electrospun nanofiber from [63].

1.2.2. Processing conditions

1.2.2.1. Voltage

Voltage is a fundamental parameter in the electrospinning process given that it determines the electrical field strength between the spinneret and the target, and controls the elongation of the jet[3]. The applied voltage is proportional to charge density on the jet. Thus, a high voltage leads to higher elongation forces exerted on the jet[32]. Whence, the voltage has an influence on the morphology and diameter of the fibers[3,32,56,65]. Megelski et al., (2002) investigated the influence of the voltage applied during electrospinning on the polystyrene (PS) fibers diameter. Their results showed that the fiber diameter decreased from about 20 to 10 μm when the voltage changed from 5 to 12 kV, with the others invariant parameters [33]. Likewise, in [32] was found that the average fiber diameter of PDLA membranes decreases from 495 nm to 403 nm with increasing voltage from 15 kV to 30

kV^{32}. Others researchers such as Deitzel et al., (2001) [65] who worked with Poly(ethylene oxide) (PEO) reported that voltage had a great repercussion in the formation of bead defects on the fibers. The fiber obtained at low voltage (5.5 kV) had a cylindrical morphology and were defect-free, but a high density of beaded fiber was found increasing the voltage above 7 kV^{65}. This behavior was confirmed by Zong et al. (2002)[56] the fiber morphology that they produced changed from a typical cylindrical shape to a beaded or string-of-pearls structure [56].

1.2.2.2.　Flow rate

Flow rate is a key parameter in controlling fiber diameter and its distribution[45]. It regulates the bulk of polymer solution ready for use in the electrospinning process[3]. When the flow rate is high, larger droplets in the needle tip are created. The results can be higher average fiber diameters[66,67] (Figure 8), beaded fiber[66] or webs instead of fibers due residual solvent which is not completely evaporated. On
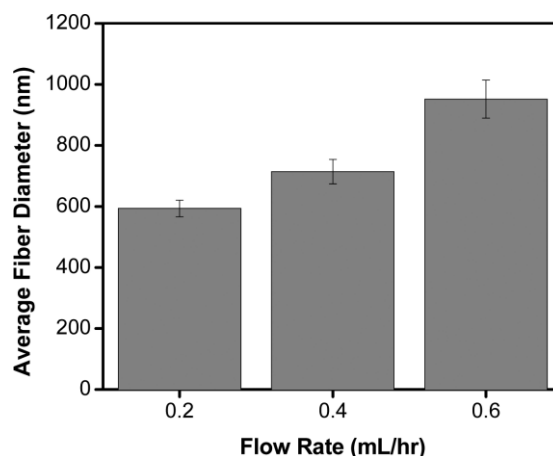
Figure 8. Effect of solution flow rate on the average fiber diameter of Nafion/PEO electrospun nanofiber mats. Electrospinning conditions: 4 kV, 5 cm SCD, 30% air RH. Solution properties: 25 wt % polymer, 99:1 wt ratio of Nafion:PEO (400 kDa MW), 1-propanol/water solvent, from [67].

the contrary, when the flow rate is low the solvent will have sufficient time for evaporation, then the process will yield uniform fibers with small diameters and without beads or with beads reduced [3,45].

Zargham et al., (2012) [45] produced fibers from nylon 6 in formic acid. They used flow rates of 0.1, 0.5, 1 and 1.5 mL/hr, a solution concentration of 20 wt%, a voltage of 20 kV and a distance from needle tip to the collector of 15 cm. They observed that at 0.5 mL/hr, was optimum flow rate which created uniform fibers, and narrowest fiber diameter distribution. At higher flow rates, the jet was unstable and tended to electrospray due to the effect of gravitational force. Also, they found other defects such as branched or splitting fibers and blobs. The SEM images can be seen in Figure 9 [45].
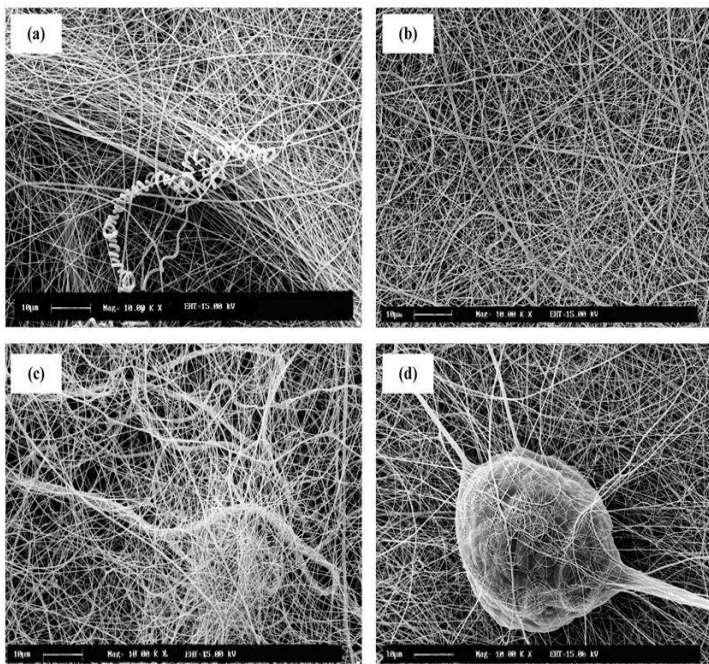
Figure 9. The SEM images of the electrospun nanofibers at various flow rates; (a) 0.1mL/hr, (b) 0.5 mL/hr, (c) 1 mL/hr, (d) 1.5 mL/hr, *from* [45].

Zong et al., (2002) [56], who reported changes in the morphology fiber from a 25 wt% PDLA solution with 1 wt% KH_2PO_4 at 20 kV varying the flow rate. They found that lower flow rate generated the smaller fibers with spindle-like beads. While for higher flow rate was observed larger fiber diameters and beads[56] (Figure 10). However, they did not study the influence of flow rate on the diameter fiber and morphology widely; and they did not reported an optimum flow even though a difference between the two flow rates is observed.
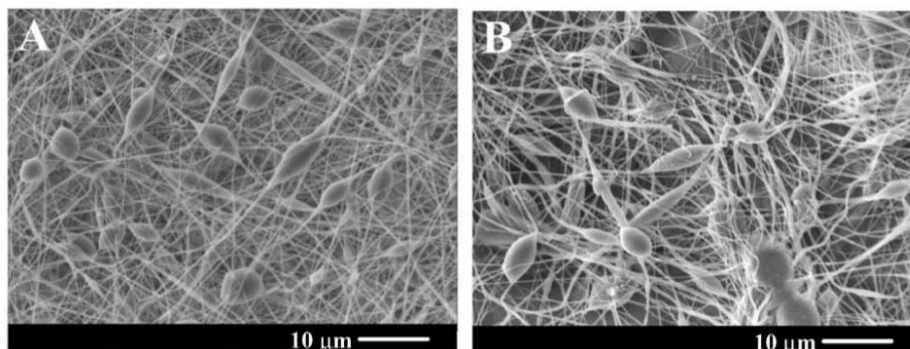
Figure 10. SEM images showing the variation of beaded fibers at different flow rate: (A) 20 ml/min; (B) 75 ml/min from [56].

The behavior described above and corroborated by several authors is not presented in all cases, for example in Figure 11 shows SEM images taken by Ribeiro et al., (2010) to fibers produced increasing the flow rate, which yields small changes in the fiber morphology, but an increase of the fiber diameter with increasing flow rate was not found [32]. For other authors such as Zhang et al., (2005) [68] the morphology fiber was only slightly changed by varying flow rate and was the least important effect of the process parameters studied [68].
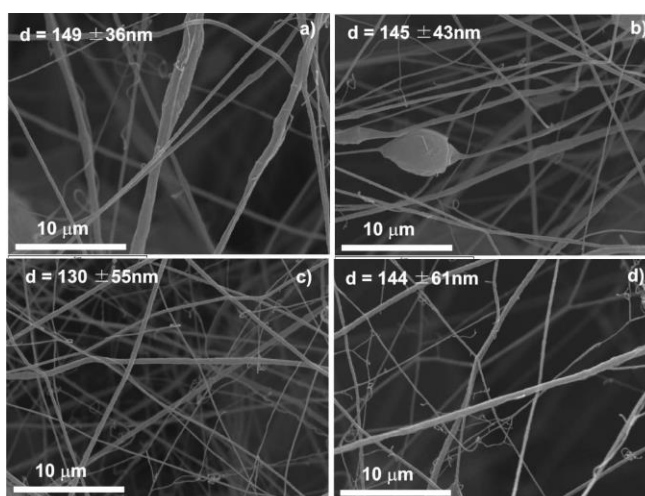
Figure 11. SEM image of PVDF electrospun nanofibers obtained from a solution of 20/80 (20% PVDF +80% DMF by w/w) at a traveling distance of 15 cm, needle diameter of 0.5 mm and voltage of 20 kV, with an increase of flow rate from 0,5 to 4 mL.h–1 (a—0,5 mL/h, b—1 m

1.2.2.3.   Distance from needle to collector

The tip to collector distance (TCD) is the space where the jet is elongated. TCD has a significant effect on jet flight time and the intensity of the electric field. If this distance is insufficient, then there is an incomplete evaporation of the solvent, whence fused fiber-fiber intersections and densely packed structure are obtained. Higher TCD decreases beads formation and mean fiber diameter. The average fiber diameter can be reduced by increasing the TCD since it increases the flying time, which leads to the greatest elongation and therefore to a thinner jet[69]. But, at a constant voltage, an increase in the TCD reduces electrostatic field strength and can produce higher mean fiber diameter or an inefficient electrospinning process [3,21,69,70]. Scarlet et al., (2012)[70] studied the influence of the TCD on the nanofiber diameter from a solution of polyetherimide in dimethylacetamide/tetrahydrofuran (DMAC/THF), their results (Figure 12) reveal that an increase of the TCD produces fibers with higher diameters[70].
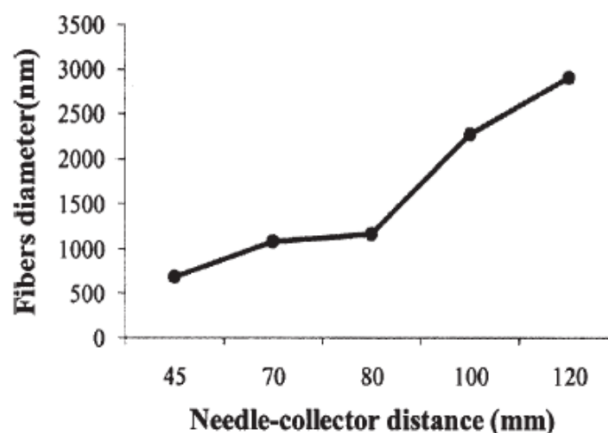
Figure 12. Correlation between the fibers diameter and the needle – collector distance (Q = 0.1mL/h, V = 30kV, syringe volume = 3 mL, needle inner diameter = 0,4 mm), from [70].

In the research accomplished by Jarusuwannapoom et al., (2005), fibrous structure from 20% (w/v) polystyrene in 1,2-dichloroethane showed beaded fibers increased with increasing TCD or with increasing applied electrostatic field (Figure 13)[71].
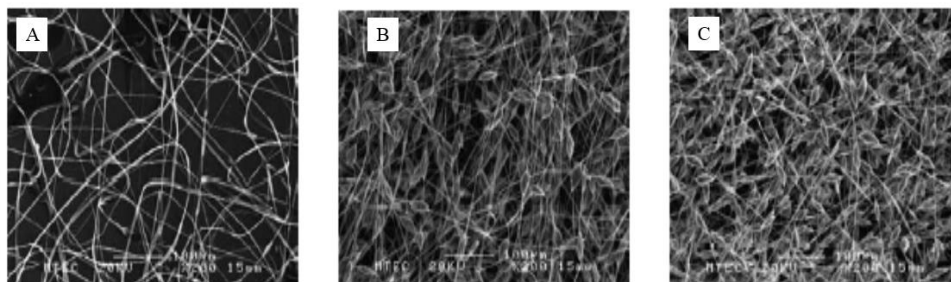
Figure 13. SEM micrographs (at 200x) of as-spun polystyrene fibers illustrating the effect of TCD. A: 7cm, B:10cm, C:15cm at V=20kV, from [71]

1.2.3. Ambient conditions

Ambient parameters such as temperature and humidity can influence fiber morphology and the efficiency of the electrospinning process [3,57]. Temperature has an effect on the solvent evaporation rate and its conductivity. In the polymer solution viscosity and surface tension as shown by Chen and Yu [72], who produced nanofibers at an elevated temperature electrospinning process. The high temperatures reduced the viscosity and surface tensions of the solutions, and increased their conductivity, which facilitated the process. They obtained a smooth surface and uniform fibers with no bead-on-a-string configurations[72].

Liang et al. (2014)[73] used the relative humidity for producing honeycomb-like 3D polymeric structures by electrospinning. They found that diameter of nanofibers decreased

suddenly from the central region to the edge region of the macrostructure at 73% relative humidity. Also, highest relative humidity yielded beaded nanofibers [73].

Elevated humidity promotes the absorption of water from polymer solution because the partial pressure of water in the atmosphere is greater. This hinders the drying process of the jet in its travel toward the target. When the humidity is very high, the result is melted fibers on the collector, which have the appearance of a transparent film. Relative humidity strongly affect the diameter fiber, but chemical nature of the polymer and solvent is crucial for producing fibers thicker or thinner [57]. Casper et al., (2004) [74] made porous electrospun fibers when carried out electrospinning in an atmosphere with more than 30% relative humidity. Also, they increased the number, diameter, shape, and distribution of the pores by increasing humidity [74].

De Vrieze et al., (2009) [57] reported smaller fiber diameters both high and low temperature using Poly(vinylpyrrolidone) dissolved in ethanol and Cellulose acetate dissolved in a mixture of acetone and N, N-dimethylacetamide. They think that maybe due to two opposing effects: evaporation rate of the solvent and viscosity of the solution. At lower temperatures the solvent is evaporated slowly. Therefore, there is a longer elongation of the jet getting smallest fiber diameter [57]. Elevated temperature cause decreasing of the viscosity will thus electric applied produce higher stretching rate and thinner fibers [57]. This effect was also showed by [75] who found the average diameter of fibers decreased slightly from about 98.3 nm at the solution temperature of 30 °C to about 89.7 nm at 60 °C; they worked with 26% w/v polyamide-6-3 solution in 85% v/v formic acid [75].

1.3. Collagen

Collagen is the main protein in mammals[27]. It is a fibrillar protein with a long and stiff triple helix structure, as shown in Figure 14. Collagen offers mechanical and physical support to tissues such as skin, bone, tendon, ligament, and other connective tissues[24,30]. It can be isolated from a variety of sources and is highly conserved and relatively nonimmunogenic[24].
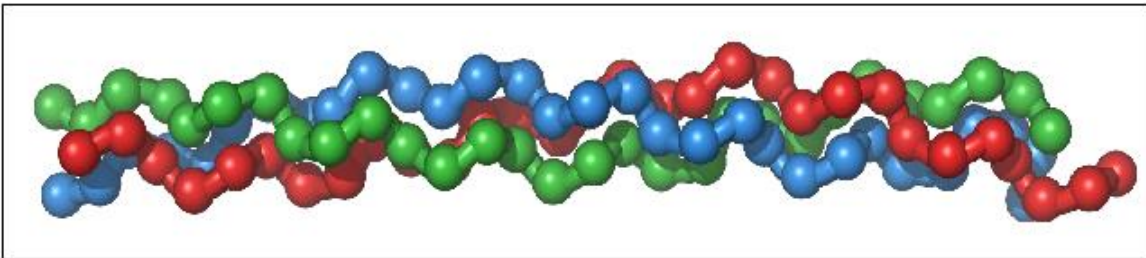
Figure 14. Collagen's triple helical structure from:
http://www.ebi.ac.uk/interpro/potm/2009_1/Protein_focus_2009_01-Collagen.html

Extracellular matrix (ECM) is mainly formed of glycosaminoglycans (GAGs) and collagen, these bridges and links to construct networks of ECM, which maintains and defines the shapes of tissue and organs especially in connective tissue [27]. In native ECM, collagen exists in a three-dimensional network structure composed of multi-fibrils in the nanofiber scale (50–500 nm) [24].

Collagen is biocompatible and biodegradable[3]. It has shown to be a good guide for cell growth and tissue repair; cells grow parallel to collagen fibers in forming a framework for aligned tissues[76], therefore, is a good substrate for tissue engineering, and it has been used in a great application in this field. Scaffolds manufactured from collagen are

promising because its signature biological and physicochemical properties are retained in in vitro preparations[29].

1.4.   Nanofibrous collagen in tissue engineering

Scaffolds for tissue engineering application should be similar both structurally and functionally to the native extracellular matrix (ECM). Materials used should be biocompatible and completely resorbable. Also, they should be three-dimensional and provide support to cell and all cellular activities such as cell differentiation. Polymers such as of lactic acid, glycolic acid, polycaprolactone, and their copolymers have been used for this objective, but they have not overcome to expectations in the clinical setting [24,26].

Since collagen is present in the native extracellular matrix and owing to its merits such as biological origin, non-immunogenicity, excellent biocompatibility and biodegradability it has been extensively used for tissue-engineering scaffolding[1,24]. Also, given that ECM is a complex of polyprotein and polysaccharide with nanofibrous porous structure[1], the fibrous scaffolds prepared from collagen via electrospinning can be architecturally similar to the collagen structure of ECM[77].

Electrospinning was utilized to produce tissue-engineering scaffolds composed of collagen nanofibers demonstrated that the structural properties of electrospun collagen vary with the tissue of origin, the isotope, and the concentration of the collagen solution [24]. In most of the studies collagen, nanofiber production utilizes hexafluoroisopropanol (HFIP) or 2,2,2-trifluoroethanol (TFE) [29] as solvents for electrospinning[30]. However, it has been

shown with non-collagenous proteins that fluoroalcohols denature not only the native structure but also lower the denaturation temperature. Additionally, electrospinning of collagen using either HFP or TFE has repeatedly been reported to yield collagen nanofibers that do not swell in aqueous media like other collagenous structures, but instead are readily soluble in water, tissue fluids or blood [29]. It has also been reported that electrospinning using HFIP transforms collagen to gelatin[30]. Research efforts are now focused on replacing HFIP with an environmentally benign solvent [30]; that does not affect the structure of collagen.

1.5. Electrospinning model

Initially, a droplet of polymer solution remains at the end of the needle due to surface tension[37]. The applied electric field induces charges in it. The interaction between surface charge and the external electric field produces a tangential stress, then the droplet becomes into a conical shape (Taylor cone)[63]. When the electric field
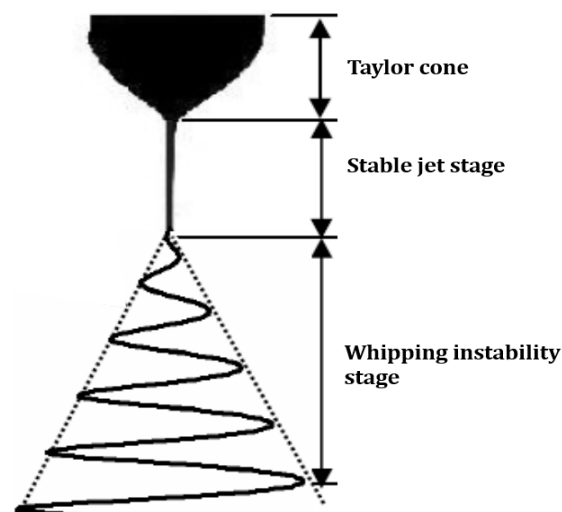
Figure 15. Behavior of the electrospun jet[88]

overcomes the surface tension fully, a fluid jet ejects from the tip of the Taylor cone [3] Here begins a stage known as stable jet stage, where the jet thins as it accelerates [78]. Before to be collected on the target, the jet undergoes a second stage referred as "whipping instability" [79] during this stage is presented bending and stretching of the jet, observed as loops of

increasing size as the instability grows [80], during its transit from the needle tip to the collector the solvent evaporates and continuous fibers are gathered on it [3]; in Figure 15 is displayed the behavior experimented by the fluid charged jet.

Feng (2002)[35], developed an one-dimensional numerical model regarding the first stage, which is crucial because contributes to the thinning directly, and establishes the conditions at the beginning of the second stage [35]. Feng's model assumes that:

- The solution is weakly conducting

- The jet carries electric charges only on its surface; any charges in the interior are quickly conducted to the surface

- The fluid is sufficiently dielectric so as to sustain an electric field tangential to the jet surface

- The radius of the jet (R) decreases slowly along the axial direction z: $dR(z)/dz \langle\langle 1$

- The fluid velocity (v) is uniform in the cross section of the jet

- All quantities depending only on the axial position z

- The model applies to Newtonian solutions

- The jet is a slender viscous object.

Table 2. Symbols used in this work

Q	Flow rate
I	Electric current
E_∞	External electric field
ε	Fluid dielectric constant
$\bar{\varepsilon}$	Air dielectric constant
ϵ_0	Permittivity of vacuum
K	Liquid conductivity
η	Viscosity
ρ	Liquid density
γ	Surface tension
g	Gravitational acceleration
R_f	Radius of fiber
R	Radius of jet
σ	Surface charge density
E	Electric field parallel to axis of jet
ν	Fluid velocity parallels to axis of jet
P	Pressure in the fluid
β	$\varepsilon/(\bar{\varepsilon}-1)$
χ	L/R_0
R_0	Characteristic radius of jet
L	Entire length of the fiber
$D_{(Ex)}$	Experimental diameter
$D_{(Pr)}$	Diameter predicted by model, $D_{(Pr)}=2R_f$

Feng (2002) applied the steady-state equations that govern the steady jet region such from the conservation of mass, conservation of charge, conservation of momentum and the Coulomb's law for the electric field. These equations are as follows (Table 2 shows the symbols used in this project):

$$\pi R^2 \upsilon = Q \qquad (1)$$

$$\pi R^2 KE + 2\pi R \upsilon \sigma = I \qquad (2)$$

$$\rho \upsilon \upsilon' = \rho g + \frac{3}{R^2}\frac{d(\eta R^2 \upsilon')}{dz} + \frac{\gamma R'}{R'} + \frac{\sigma \sigma'}{\bar{\varepsilon}} + (\varepsilon - \bar{\varepsilon})EE' + \frac{2\sigma E}{R} \tag{3}$$

$$E = E_\infty - \ln \chi \left(\frac{d(\sigma R)}{dz} - \frac{\beta}{2}\frac{d^2(ER^2)}{dz^2} \right) \tag{4}$$

Feng (2002) proposed the scales below to obtain the equations in a dimensionless form:

$$\upsilon_0 = \frac{Q}{\pi R_0^2}$$

$$E_0 = \frac{I}{\pi R_0^2 K}$$

$$\sigma_0 = \overline{\varepsilon E}$$

Near the end of the steady jet region, the tangential electrical forces ($2\sigma E/h$) govern the acceleration of the jet, so, the equation 3 is reduced to:

$$\rho \upsilon \upsilon' = \frac{2\sigma E}{R} \tag{5}$$

The convective current contributes mostly to the total current in the steady jet region, thus:

$$\sigma = \frac{I}{2\pi R \upsilon} \tag{6}$$

Using Equations (1), (5) and (6), it yields:

$$\frac{1}{R^5}\frac{dR}{dz} = -\frac{\pi^2 IE_\infty}{\rho Q^3} \quad \text{or} \quad R = \left(\frac{\pi^2 IE_\infty z}{\rho Q^3}\right)^{-1/4} \tag{7}$$

This author [81] demonstrated a similar scaling expression. The equation (7) has been derived to predict the radius of the jet at the end of the region of the steady jet; however, that expression can be used for obtaining the radius of fiber, given the fact that it showed to predict with acceptable accuracy experimental radius [21,59].

Using L and R_f as new characteristics scaling for z and R, it yields:

$$R_f = \left(\frac{\pi^2 IE_\infty L}{\rho Q^3}\right)^{-1/4} \tag{8}$$

The corresponding new scale for E, v and σ are:

$$E = \frac{\Delta V}{L}$$

$$\upsilon_f = \frac{Q}{\pi R_f^2} = \left[\frac{I(\Delta V)}{\pi^2 \rho Q}\right]^{1/2}$$

$$\sigma_f = \frac{I}{2\pi R_f V_f} = \frac{R_f I}{2Q}$$

I (electric current) was not measured in the lab. Thus, this analysis uses an already proposed scaling [82] for current in electrospinning:

$$I \approx EK^{0.4}Q^{0.5} \tag{9}$$

Substituting for E and I, the scaled radius (R_f) is:

$$R_f \approx \left(\frac{\pi^2 (\Delta V)^2 K^{2/5}}{\rho L Q^{5/2}} \right)^{-1/4} \tag{10}$$

Gadkari (2014)[36] accomplished the preceding expression.

Equation 10 can be rewritten as follows, doing *V, K, L,* and ρ constant values:

$$R_f \approx \left(C \frac{1}{Q^{5/2}} \right)^{-1/4} \approx \left(C Q^{5/8} \right)$$

Where $C \approx \left(\frac{\pi^2 (\Delta V)^2 K^{2/5}}{\rho L} \right)^{-1/4}$, which is a constant.

Now $D_{(Pr)} \approx 2R_f$ (11)

2. METHODS

Fiber production by electrospinning process

The solution was prepared by dissolving collagen in acetic acid (90% v/v in water) to a final concentration of 20% w/v, its density was 1094 kg/m^3. We assumed that the conductivity of the solution is in the order of 1 µS/cm, considering that the solution was prepared with milli-Q water and glacial acetic acid and that the collagen has a weak positive charge. This solution was stirred for 3 hours at 60 °C, and then at room temperature for 33 hours. The process electrospinning was carried
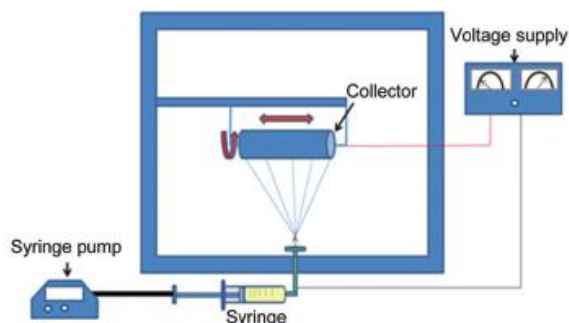
Figure 16. Schematic of the electrospinning process

out on an electrospinning equipment (Figure 16) that consist of a power supply (GAMMA, Ormond Beach, FL), an injection pump (New Era, Farmingdale, NY), a rotating drum, a 3 mL Luer-lock syringe (BDTM, VWR INTERNATIONAL), and a 23 gauge capillary steel needle of 1.5 inches in length (CML Supply). The collagen solution was loaded into a plastic 3 mL syringe connected to a capillary blunt type steel needle. The syringe was placed in the syringe pump and the needle underneath the grounded rotating drum collector at a distance of 10 cm. The rotating drum velocity was maintained at 1554 rpm. The positive pole of the high-voltage power supply was connected to the needle and the negative pole to the rotating drum. The production of nanofibers was obtained by the action of the induced voltage and injection pump, which pushed the solution. The experimental

setup for the study of the effect of voltage and flow rate on the nanofiber diameter was as follows: each experiment was performed at 20 °C with a relative humidity from 50 to 60%. The electrospinning process was carried out at voltages of 30, 35, 40 and 45 kV. The solutions were fed at rates of 1, 3, 5 and 7 mL/h. Therefore, the independent variables were flow rate and voltage. Since they can be manipulated to obtain the fiber diameter, which was the response or dependent variable. It is important to know fiber diameter because it is strongly correlated with mechanical properties of fibers and it determines cell morphology, phenotype, and differentiation[34]. The fibers were collected on rectangular aluminum screens, which were used as targets. Electrospun collagen fiber mats were stored in clean paper bags at 20°C inside a desiccator until scanning electron microscopy (SEM) analysis was performed.

Statistical analysis of the data

A 4^2 factorial design was carried out because there are two factors at four levels; each combination of voltage and flow rate was conducted in triplicate, and all 48 tests were run in random order. Two-way ANOVA method was used to evaluate the significant difference between these data at the 0.05 level of confidence. The analysis was performed using the software Minitab.

Obtaining scanning electron microscopy images

Scanning Electron Microscopy (SEM) Nanofiber morphology was observed on a JEOL JSM-6390 scanning electron microscope operated at 5 keV. The nanofibers were

coated with gold using a Denton Vacuum Desk IV sputter coater to improve the conductivity of the samples and thus the quality of the SEM images.

Fiber diameter determination with DiameterJ

Micrographs from the SEM were digitized and analyzed using the DiameterJ plug-in in ImageJ 1.47v (National Institutes of Health, USA) to determine the average fiber diameters. On February 2015, Nathan Hotaling of National Institute of Standards and Technology released the first version of DiameterJ publicly and on May 2015 it was available online the article in which this tool was validated [34].

Prediction of the fiber diameter

In this section, the results of fiber diameter, D, with the flow rate, Q, are presented, for elucidating the *D* dependence of *Q*. The fiber diameters represent an average of all the voltages considered in this study and the number of replicas under same conditions, considering the little dependence of the fiber diameter with the applied electric voltage, as demonstrated via ANOVA.

For plotting purposes the log (D) vs. the log (Q) is used with the aim of finding the exponent that relates D with the Q by applying the properties of logarithms with base 10.

$$Log_{10}D_{(Ex)} = mLog_{10}Q + b \qquad\qquad (12)$$

$$D_{(Ex)} = 10^b Q^m \ \text{Or} \ D_{(Ex)} = C_{Ex} Q^m \tag{13}$$

Where $C_{Ex,}$ is a constant.

The average prediction error of the chosen analytical model was measured using the following equation:

$$\delta = \frac{100}{n} \times \sum_{i=1}^{n} \left| \frac{D_{i,Ex} - D_{i,Pr}}{D_{i,Pr}} \right|, \tag{14}$$

Where $D_{i,\ Ex}$ is measured diameter corresponding to i_{th} trial; $D_{i,\ Pr}$ is predicted diameter corresponding to i_{th} trial and n is the number of trials.

3. RESULTS

Fiber production by electrospinning process

In general, fibers display a uniform morphology with no beads-like defects, such as image display in Figure 17.
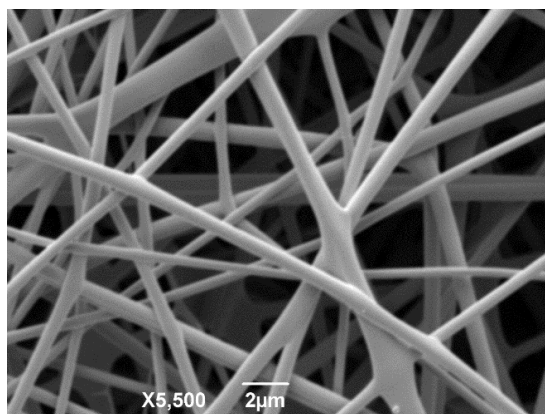
Figure 17. SEM image of collagen fiber

Statistical analysis of the data

The tool used for obtaining the average diameters was able of to count between 7,297 and 139,574 data points per image with a mean count of 47,296.6, which provides a high level of confidence in fiber diameter measurements. In the results, there was an outlier at $Q = 5mL/h$ and $V = 30$ kV that is $D = 840.01nm$; this value was removed to prevent a distorted analysis of variance. The outlier may be due to fiber swelling caused by moisture dsorption. The ANOVA is summarized in Table 3, based on both F and P values, it was inferred that flow rate significantly effects the fiber diameter while voltage has weak influence over it. Also, there is no evidence of a combined effect between these factors.

The histogram (Figure 18C) and normal probability plot (Figure 18A) show that data fits a normal distribution. The residuals versus fitted values plot (Figure 18B) and residuals versus observation order plot shows that the errors don't have a pattern, they are scattered randomly which means that they are independent.

Table 3. Analysis of Variance for Diameter (nm), using Adjusted SS for Tests

Source of variation	Degrees Freedom	Sum of Squares Adjusted	Mean Squares Adjusted	F-Ratio	P-Value
Voltage	3	29764	9921	1.46	0.244
Flow rate	3	89646	29882	4.41	0.011
Interaction	9	93788	10421	1.54	0.179
Error	31	210188	6780		
Total	46	422536			
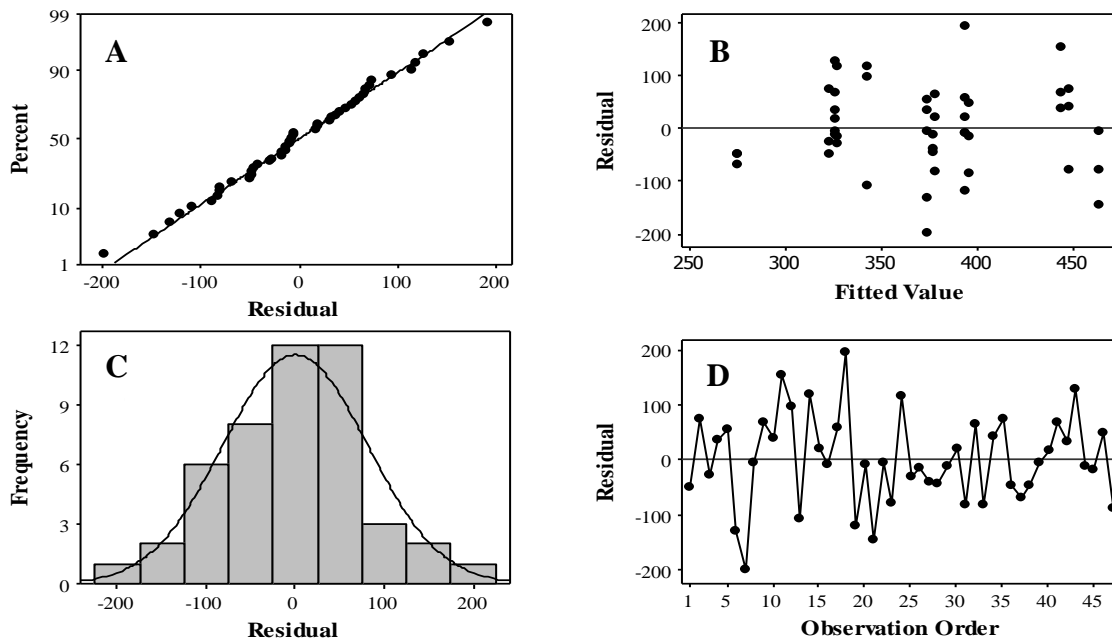
Figure 18. Residual plots for Fiber Diameter (nm). A: Normal probability plot; B: Versus fits; C: Histogram; D: Versus order

Relationship between flow rate and fiber diameter

The results of the study of the influence of the flow rate on the diameter of the nanofibers are given in Figure 19, where we can notice an increase of the average fiber diameter with the increase of the flow rate, from 317 ± 69 to 438 ± 72 nm in the range of voltages used in the experiments. Likewise, Figure 20 displays the SEM images obtained from fibers at some voltage and all flow rates. It is clearly noticed the behavior above exposed. This behavior has been previously observed in other research works using synthetic polymers.[21,33,56,83] Megelski and colleagues investigated the effects of flow rate on the structure of electrospun fibers from a polystyrene/tetrahydrofuran solution.[33] They observed that fiber diameter increased with increasing flow rate. When the flow rate is high, larger droplets are produced at the end of the capillary causing the jet solution to be electrosprayed without any sufficient elongation, because the electric field strength is not capable of stretching the ejected solution. Therefore, thicker fibers are obtained[45]. But Riverio et al., did not found that behavior, they worked with Poly(vinylidene fluoride) (PVDF) dissolved in N, N-Dimethyl Formamide (DMF) with a concentration of 20% (w/w) of PVDF, at a traveling distance of 15 cm, and voltage of 20 kV, with an increase of flow rate from 0,5 to 4 mL/h. Contradictory results shown in the literature about this point are reasonable due there are so others factors that effect the diameter size, such as solution properties, processing conditions and ambient conditions which each researcher have set up differently.
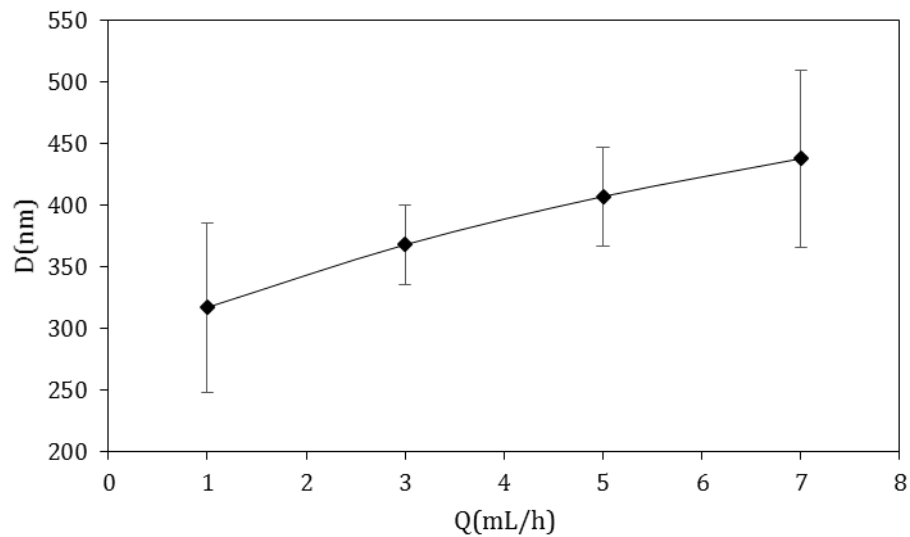
Figure 19. Mean Diameter vs. Flow rate. The error bars represent the standard deviations. The line is drawn as a guide to the eye.
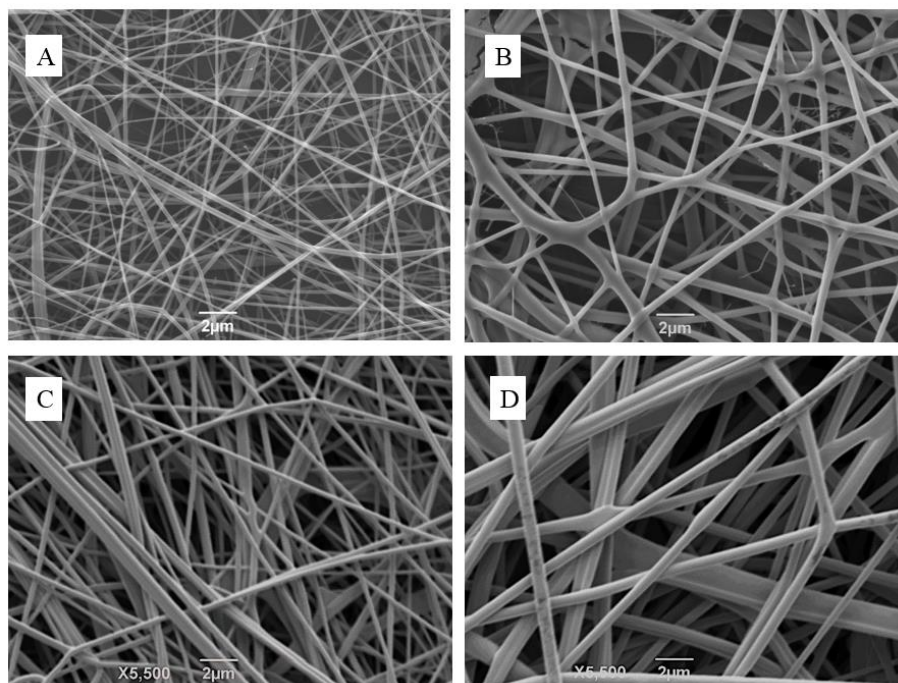
Figure 20. SEM images of collagen fibers at V=45kV A. Q=1mL/h, B. Q=3mL/h, C.Q=5mL/h, D. Q=7mL/h.

Relationship between voltage and fiber diameter

Regarding the study of the influence of the voltage on the diameter of the nanofibers, the experimental results show that the diameter of the nanofibers decreases with the increasing applied voltage, with average values of 418 ± 95, 399 ± 20, 382 ± 53 and 331 ± 75 nm for voltages of 30, 35, 40 and 45kV (Figure 21). The effect of voltage on diameter is not as pronounced as flow rate, but it is observed that there is an important reduction on it, like it is shown in Figure 22. The above results show that the amount of charge existing on the jet determines the diameter of the deposited nanofibers. An increase in applied voltage gives rise to high electric field on the surface of the solution drop at the needle tip. This allows greater elongation of the solution drop due to the presence of major Coulomb force in the jet and a strong electric field. Thereby, the jet diameter decreases during the elongation process, and fiber becomes very thin[59,84,85]. However, in some cases no clear effect of the applied voltage in the fiber diameter, such as is the case of Ribeiro et al., who found an influence "quite modest." They observed that the average fiber diameter of the polymeric electrospun membranes decreased from 495 nm to 403 nm with increasing voltage from 15 kV to 30 kV.
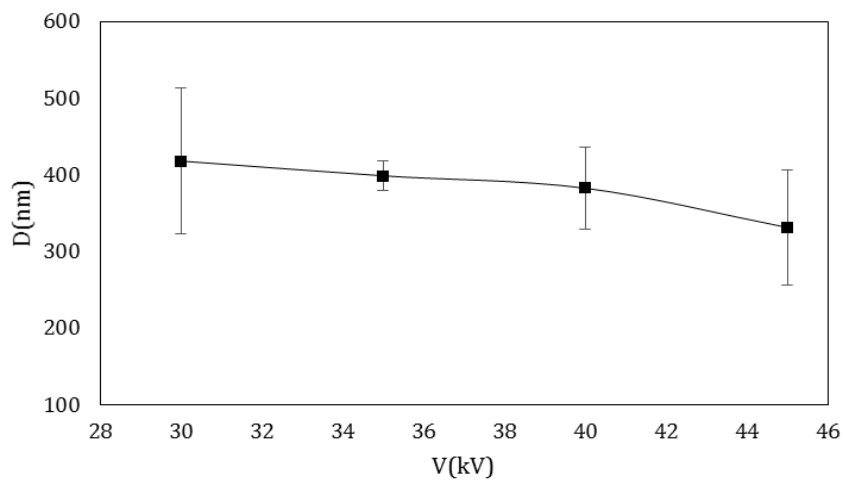
Figure 21. Mean Diameter vs. Voltage. The error bars represent the standard deviations. The line is drawn as a guide to the eye.
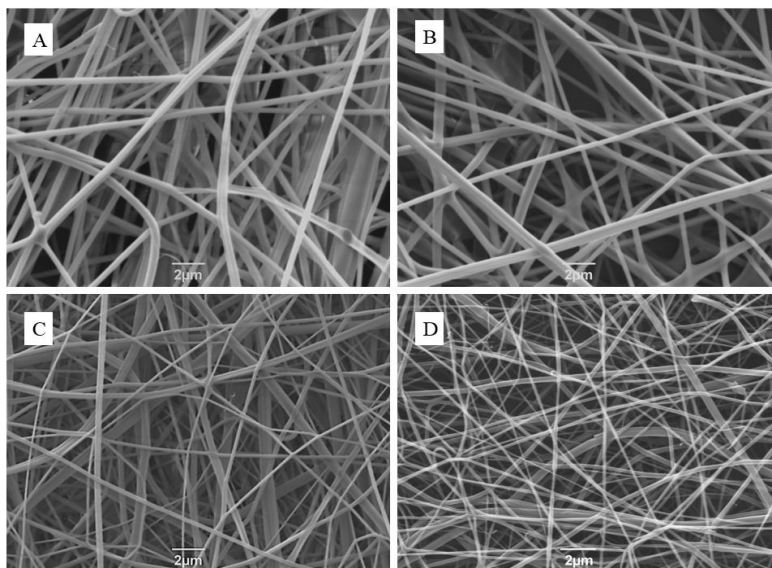
Figure 22. SEM images of collagen fibers at Q=1mL/h A.V=30kV, B. V=35kV, C. V=40kV, D. V=45kV.

Prediction of the fiber diameter
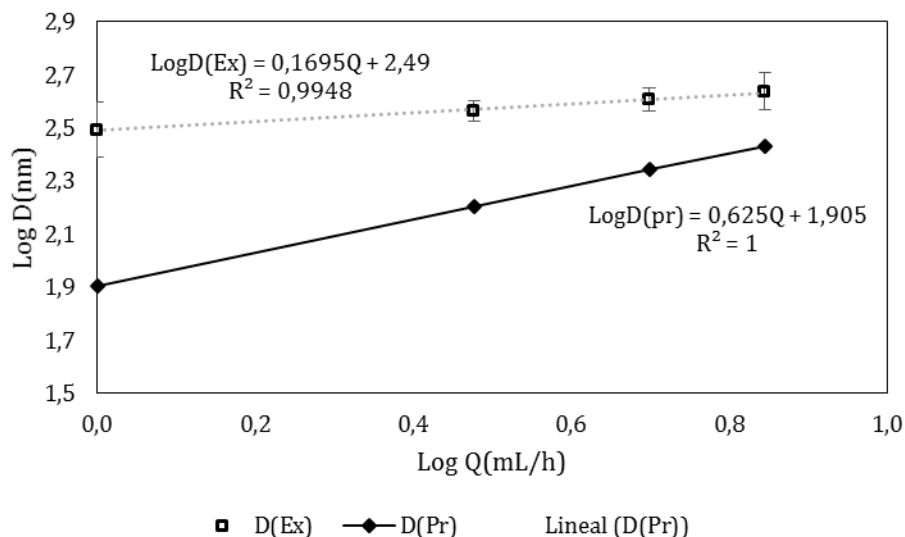
Figure 23. The Log D vs Log Q. Experimental data compared to theoretical data.

The average fiber diameter versus the flow rate in logarithm scale is presented in Figure 23; open symbols and the solid line represent the experimental and theoretical results, respectively. Those values are a mean of the obtained diameters for all voltages used in this study. The theoretical data was obtained with equation [11]. Note that the experimental results are slightly greater that the theoretical by a factor that ranges from 1.1 to 1.3. Similarly, Rutledge et al. (2002)[86], found that their theoretical curve was shifted below the experimental data by roughly a factor of 2. They evaluated a model for predicting the terminal diameter of fibers. Linear regression resulted in a slope close to 1/6 for experimental data. This result is an acceptable agreement with the predicted slope of 5/8, considering that there are no fitting parameters in the theory neither correcting for solvent evaporation.

The model predicts the fiber diameter with an average error (equation [14]) of 16.75% with 16 sets of experimental data. Fridrikh et al., (2003) used a different scaling law to find an expression for predicting the fiber diameter at the collector. They used polyethylene oxide (PEO) and polyacrylonitrile (PAN) that model predicted of fiber diameter with errors of 10% and 20% respectively, in a limited range of fiber diameters. It is important to note that the equation [9] was used to scale the current *(I).* This scaling was proposed by Bhattacharjee et al., (2010) who theorized that during electrospinning process takes place simultaneously a polymer-rich main jet and an electrospraying of solvent-rich droplets. They affirm that total current have two components one of which is present in the main jet and the other on the electrospray, they named to the second component as a "leakage current" due removes charges from the main jet. But they used linear homopolymers in nonaqueous solvents in their study, while, the current on our system may have a more complicated behavior. This implies that the used expression for obtaining the theoretical data might incur in an erroneous estimation of the transported total current by the jet, which impacts in the fiber diameter. Also, one should keep in mind that there are other parameters that influence the fiber diameter such as humidity, surface tension, chemical nature of solution, which are not taken into account in this model.

From linear regression (Figure 23) it was found that the experimental data can be represented by the following equation: $D_{(Ex)} = 309.03Q^{1/6}$

4. CONCLUDING REMARKS

In this project nanofibers from collagen dissolved in acetic acid were produced, the relationship between flow rate and the voltage on the fiber diameter was determined, and a prediction model of the fiber diameter was identified. Also, an expression for the fiber diameter as function of flow rate was obtained. The results are summarized as follows:

1. Fibers presented a uniform morphology, with no defects and random distribution.

2. DiameterJ counted over 47,000 points per image on average, which provides a high level of confidence in fiber diameter measurements.

3. The flow rate significantly effects the fiber diameter. There is an increase of the average fiber diameter from 317 ± 69 to 438 ± 72 with the increase of the flow rate from 1 to 7 mL/h

4. The voltage has weak influence over the fiber diameter, at the process conditions to which experimental trials were carried out. The diameter of the nanofibers decreases from 418 ± 95 to 331 ± 75 nm increasing applied voltage from 30 to 45 kV

5. The identified model predicts the fiber diameter with an average error of 16.75%

6. The experimental data can be represented by: $D_{(Ex)} = 309.03 Q^{1/6}$

5. REFERENCES

1.   Chen Z, Mo X, He C, Wang H. Intermolecular interactions in electrospun collagen-chitosan complex nanofibers. *Carbohydr Polym*. 2008;72(3):410-418. doi:10.1016/j.carbpol.2007.09.018.

2.   Wu Y, Yu JY, He JH, Wan YQ. Controlling stability of the electrospun fiber by magnetic field. *Chaos, Solitons and Fractals*. 2007;32(1):5-7. doi:10.1016/j.chaos.2006.05.023.

3.   Ghorani B, Tucker N. Fundamentals of electrospinning as a novel delivery vehicle for bioactive compounds in food nanotechnology. *Food Hydrocoll*. 2015;51:227-240. doi:10.1016/j.foodhyd.2015.05.024.

4.   Kucinska-Lipka J, Gubanska I, Janik H, Sienkiewicz M. Fabrication of polyurethane and polyurethane based composite fibres by the electrospinning technique for soft tissue engineering of cardiovascular system. *Mater Sci Eng C*. 2015;46:166-176. doi:10.1016/j.msec.2014.10.027.

5.   Castillo-Ortega MM, Montaño-Figueroa a. G, Rodríguez-Félix DE, et al. Preparation by coaxial electrospinning and characterization of membranes releasing (−) epicatechin as scaffold for tissue engineering. *Mater Sci Eng C*. 2015;46:184-189. doi:10.1016/j.msec.2014.10.031.

6.   Ahn H, Ju YM, Takahashi H, et al. Engineered small diameter vascular grafts by combining cell sheet engineering and electrospinning technology. *Acta Biomater*. 2015;16:14-22. doi:10.1016/j.actbio.2015.01.030.

7.   Walser J, Ferguson SJ. Oriented nanofibrous membranes for tissue engineering applications: Electrospinning with secondary field control. *J Mech Behav Biomed Mater*. 2015:1-11. doi:10.1016/j.jmbbm.2015.06.027.

8.   Atila D, Keskin D, En Tezcaner A. Cellulose acetate based 3-dimensional electrospun scaffolds for skin tissue engineering applications. *Carbohydr Polym*. 2015;133:251-261. doi:10.1016/j.carbpol.2015.06.109.

9.   Gautam S, Dinda AK, Mishra NC. Fabrication and characterization of PCL/gelatin composite nanofibrous scaffold for tissue engineering applications by

electrospinning method. *Mater Sci Eng C Mater Biol Appl*. 2013;33(3):1228-1235. doi:10.1016/j.msec.2012.12.015.

10. Shen L, Yu X, Cheng C, et al. High fi ltration performance thin fi lm nano fi brous composite membrane prepared by electrospraying technique and hot-pressing treatment. *J Memb Sci*. 2016;499:470-479.

11. Kiani S, Mahmoud S, Shahtahmassebi N, Saljoughi E. Applied Surface Science Hydrophilicity improvement in polyphenylsulfone nanofibrous filtration membranes through addition of polyethylene glycol. *Appl Surf Sci*. 2015;359:252-258.

12. Arribas P, Khayet M, García-Payo MC, Gil L. Self-sustained electro-spun polysulfone nano-fibrous membranes and their surface modification by interfacial polymerization for micro- and ultra-filtration. *Sep Purif Technol*. 2014;138:118-129. doi:10.1016/j.seppur.2014.10.010.

13. Kim HC, Choi BG, Noh J, Song KG, Lee SH, Maeng SK. Electrospun nanofibrous PVDF-PMMA MF membrane in laboratory and pilot-scale study treating wastewater from Seoul Zoo. *Desalination*. 2014;346:107-114. doi:10.1016/j.desal.2014.05.005.

14. Formo E, Camargo PHC, Lim B, Jiang M, Xia Y. Functionalization of ZrO2 nanofibers with Pt nanostructures: The effect of surface roughness on nucleation mechanism and morphology control. *Chem Phys Lett*. 2009;476(1-3):56-61. doi:10.1016/j.cplett.2009.05.075.

15. Koo W, Choi S, Kim N, Jang J, Kim I. Sensors and Actuators B : Chemical Catalyst-decorated hollow WO 3 nanotubes using layer-by-layer self-assembly on polymeric nanofiber templates and their application in exhaled breath sensor. *Sensors Actuators B Chem*. 2016;223:301-310.

16. Zhang Y, Liu S, Li Y, et al. Biosensors and Bioelectronics Electrospun graphene decorated MnCo 2 O 4 composite nano fi bers for glucose biosensing. *Biosens Bioelectron*. 2015;66:308-315.

17. Wu J, Yin F. Sensitive enzymatic glucose biosensor fabricated by electrospinning composite nanofibers and electrodepositing Prussian blue film. *J Electroanal Chem*. 2013;694:1-5. doi:10.1016/j.jelechem.2013.02.003.

18. Wang W, Zhang L, Tong S, Li X, Song W. Three-dimensional network films of electrospun copper oxide nanofibers for glucose determination. *Biosens Bioelectron*. 2009;25(4):708-714. doi:10.1016/j.bios.2009.08.013.

19. Marx S, Jose M V, Andersen JD, Russell AJ. Electrospun gold nanofiber electrodes for biosensors. *Biosens Bioelectron*. 2011;26(6):2981-2986. doi:10.1016/j.bios.2010.11.050.

20. Gi I, Lee J, Rajan A, Park C, Sang C. A comprehensive electric field analysis of cylinder-type multi-nozzle electrospinning system for mass production of nanofibers. *J Ind Eng Chem*. 2015;31:251-256. doi:10.1016/j.jiec.2015.06.033.

21. Cramariuc B, Cramariuc R, Scarlet R, Manea LR, Lupu IG, Cramariuc O. Fiber diameter in electrospinning process. *J Electrostat*. 2013;71(3):189-198. doi:10.1016/j.elstat.2012.12.018.

22. Liu Y, Ma Q, Yang M, et al. Flexible hollow nanofibers : Novel one-pot electrospinning construction , structure and tunable luminescence – electricity – magnetism trifunctionality. *Chem Eng J*. 2016;284:831-840.

23. Chen ZG, Wang PW, Wei B, Mo XM, Cui FZ. Electrospun collagen-chitosan nanofiber: a biomimetic extracellular matrix for endothelial cell and smooth muscle cell. *Acta Biomater*. 2010;6(2):372-382. doi:10.1016/j.actbio.2009.07.024.

24. Rho KS, Jeong L, Lee G, et al. Electrospinning of collagen nanofibers: effects on the behavior of normal human keratinocytes and early-stage wound healing. *Biomaterials*. 2006;27(8):1452-1461. doi:10.1016/j.biomaterials.2005.08.004.

25. Sell SA, McClure MJ, Garg K, Wolfe PS, Bowlin GL. Electrospinning of collagen/biopolymers for regenerative medicine and cardiovascular tissue engineering. *Adv Drug Deliv Rev*. 2009;61(12):1007-1019. doi:10.1016/j.addr.2009.07.012.

26. Matthews JA, Wnek GE, Simpson DG, Bowlin GL. Electrospinning of Collagen Nanofibers. *Biomacromolecules*. 2002;1(Iii):232-238.

27. Ping S, Eong W, Zhu X, Beuerman R. Development of a novel collagen – GAG nanofibrous scaffold via electrospinning. *Mater Sci Eng C Mater Biol Appl*.

2007;27:262-266. doi:10.1016/j.msec.2006.05.010.

28. Buttafoco L, Kolkman NG, Engbers-Buijtenhuijs P, et al. Electrospinning of collagen and elastin for tissue engineering applications. *Biomaterials*. 2006;27(5):724-734. doi:10.1016/j.biomaterials.2005.06.024.

29. Zeugolis DI, Khew ST, Yew ESY, et al. Electro-spinning of pure collagen nano-fibres – Just an expensive way to make gelatin? *Biomaterials*. 2008;29(15):2293-2305. doi:10.1016/j.biomaterials.2008.02.009.

30. Chakrapani VY, Gnanamani a., Giridev VR, Madhusoothanan M, Sekaran G. Electrospinning of type I collagen and PCL nanofibers using acetic acid. *J Appl Polym Sci*. 2012;125(4):3221-3227. doi:10.1002/app.36504.

31. Castilla Casadiego D, Ramos Avilez H V, Herrera-Posada S, et al. Engineering of a stable collagen nanofibrous scaffold with tunable fiber diameter, alignment, and mechanical properties. *Macromol MaterEng*. 2016;Submitted:1-12. doi:10.1002/mame.201600156.

32. Ribeiro C, Sencadas V, Ribelles JLG, Lanceros-Méndez S. Influence of Processing Conditions on Polymorphism and Nanofiber Morphology of Electroactive Poly(vinylidene fluoride) Electrospun Membranes. *Soft Mater*. 2010;8(3):274-287. doi:10.1080/1539445X.2010.495630.

33. Megelski S, Stephens JS, Chase DB, Rabolt JF. Micro- and Nanostructured Surface Morphology on Electrospun Polymer Fibers. *Macromolecules*. 2002;35(22):8456-8466. doi:10.1021/ma020444a.

34. Hotaling N a, Bharti K, Kriel H, Simon CG. DiameterJ: A validated open source nanofiber diameter measurement tool. *Biomaterials*. 2015;61:327-338. doi:10.1016/j.biomaterials.2015.05.015.

35. Feng JJ. The stretching of an electrified non-Newtonian jet: A model for electrospinning. *Phys Fluids*. 2002;14(11):3912-3926. doi:10.1063/1.1510664.

36. Gadkari SB. Scaling analysis for electrospinning. *Springerplus*. 2014;3:705. doi:10.1186/2193-1801-3-705.

37. Jiang T, Carbone EJ, Lo KW-H, Laurencin CT. Electrospinning of Polymer

Nanofibers for Tissue Regeneration. *Prog Polym Sci*. 2015;46:1-24. doi:10.1016/j.progpolymsci.2014.12.001.

38.   Formhals A. Process and apparatus for preparing artificial threads. 1934. http://www.google.com/patents/US1975504?hl=es.

39.   Formhals A. Method and apparatus for spinning. 1939.

40.   Formhals A. Artificial thread and method of producing same. 1940.

41.   Sill TJ, von Recum H a. Electrospinning: applications in drug delivery and tissue engineering. *Biomaterials*. 2008;29(13):1989-2006. doi:10.1016/j.biomaterials.2008.01.011.

42.   Taylor G, Society TR, Society R, Sciences P. Disintegration of Water Drops in an Electric Field. *Proc R Soc A Math Phys Eng Sci*. 1964;280(1382):383-397. doi:10.1098/rspa.1964.0151.

43.   Taylor G. Electrically Driven Jets. *Proc R Soc London, Ser A, Math Phys Sci*. 1969;313:453-475.

44.   Liu L, Dzenis Y. Simulation of electrospun nanofibre deposition on stationary and moving substrates. *Micro Nano Lett*. 2011;6(6):408. doi:10.1049/mnl.2011.0167.

45.   Zargham S, Bazgir S, Tavakoli A, Rashidi AS, Damerchely R. The Effect of Flow Rate on Morphology and Deposition Area of Electrospun Nylon 6 Nanofiber. *J Eng Fiber Fabr*. 2012;7(4):42-49.

46.   Shields KJ, Beckman MJ, Bowlin GL, Wayne JS. Mechanical properties and cellular proliferation of electrospun collagen type II. *Tissue Eng*. 2004;10(9):1510-1517. doi:10.1089/ten.2004.10.1510.

47.   Jeong SI, Krebs MD, Bonino CA, Samorezov JE, Khan SA, Alsberg E. Electrospun chitosan-alginate nanofibers with in situ polyelectrolyte complexation for use as tissue engineering scaffolds. *Tissue Eng Part A*. 2011;17(1-2):59-70. doi:10.1089/ten.TEA.2010.0086.

48.   Ahmed FE, Lalia BS, Hashaikeh R. A review on electrospinning for membrane fabrication: Challenges and applications. *Desalination*. 2015;356:15-30. doi:10.1016/j.desal.2014.09.033.

49.   Tan L, Hu J, Zhao H. Design of bilayered nano fi brous mats for wound dressing using an electrospinning technique. *Mater Lett*. 2015;156:46-49.

50.   Zhao R, Li X, Sun B, et al. Electrospun chitosan/sericin composite nanofibers with antibacterial property as potential wound dressings. *Int J Biol Macromol*. 2014;68:92-97. doi:10.1016/j.ijbiomac.2014.04.029.

51.   Balogh A, Cselkó R, Démuth B, Verreck G, Mensch J. Alternating current electrospinning for preparation of fi brous drug delivery systems. *Int J Pharm*. 2015;495:75-80.

52.   Hu X, Liu S, Zhou G, Huang Y, Xie Z, Jing X. Electrospinning of polymeric nanofibers for drug delivery applications. *J Control Release*. 2014;185(1):12-21. doi:10.1016/j.jconrel.2014.04.018.

53.   Chen H, Liu Y, Hu Q. A novel bioactive membrane by cell electrospinning. *Exp Cell Res*. 2015;338:261-266. doi:10.1016/j.yexcr.2015.08.007.

54.   Zhang H, Fu Q-W, Sun T-W, et al. Amorphous calcium phosphate, hydroxyapatite and poly(d,l-lactic acid) composite nanofibers: Electrospinning preparation, mineralization and in vivo bone defect repair. *Colloids Surf B Biointerfaces*. 2015;136:27-36. doi:10.1016/j.colsurfb.2015.08.015.

55.   Braghirolli DI, Steffens D, Pranke P. Electrospinning for regenerative medicine: A review of the main topics. *Drug Discov Today*. 2014;19(6):743-753. doi:10.1016/j.drudis.2014.03.024.

56.   Zong X, Kim K, Fang D, Ran S, Hsiao BS, Chu B. Structure and process relationship of electrospun bioabsorbable nanofiber membranes. *Polymer (Guildf)*. 2002;43(16):4403-4412. doi:10.1016/S0032-3861(02)00275-6.

57.   De Vrieze S, Van Camp T, Nelvig a., Hagstr??m B, Westbroek P, De Clerck K. The effect of temperature and humidity on electrospinning. *J Mater Sci*.

2009;44(5):1357-1362. doi:10.1007/s10853-008-3010-6.

58.   Liu Y, Ma G, Fang D, Xu J, Zhang H, Nie J. Effects of solution properties and electric field on the electrospinning of hyaluronic acid. *Carbohydr Polym*. 2011;83(2):1011-1015. doi:10.1016/j.carbpol.2010.08.061.

59.   Rutledge GC, Li Y, Fridrikh S, Warner SB, Kalayci VE, Patra P. Electrostatic Spinning and Properties of Ultrafine Fibers. *Natl Text Cent Annu Rep Novemb 2001M01-D22*. 2001;(November):1-10.

60.   Angammana CJ, Jayaram SH. Analysis of the effects of solution conductivity on electrospinning process and fiber morphology. *IEEE Trans Ind Appl*. 2011;47(3):1109-1117. doi:10.1109/TIA.2011.2127431.

61.   Fong H, Fong H, Chun I, Chun I, Reneker D, Reneker D. Beaded nano bers formed during electrospinning. *Polymer (Guildf)*. 1999;40:4585-4592.

62.   Huang CB, Chen SL, Lai CL, et al. Electrospun polymer nanofibres with small diameters. *Nanotechnology*. 2006;17:1558-1563. doi:10.1088/0957-4484/17/6/004.

63.   Wang S, He J, Xu L. Non-ionic surfactants for enhancing electrospinability and for the preparation of electrospun nanofiber. *Polym Int*. 2008;57(May):171-180. doi:10.1002/pi.

64.   Liu Y, Ren Z, Wang S. Theoretical Analysis and Experimental Verification of the Effect of Surface Tension on Morphology of Nanofibers in Bubble Electrospinning. *Int J Nonlinear Sci Numer Simul*. 1882;11(8):625-630.

65.   Deitzel J., Kleinmeyer J, Harris D, Beck Tan N. The effect of processing variables on the morphology of electrospun nanofibers and textiles. *Polymer (Guildf)*. 2001;42(1):261-272. doi:10.1016/S0032-3861(00)00250-0.

66.   Zhang C, Yuan X, Wu L, Han Y, Sheng J. Study on morphology of electrospun poly(vinyl alcohol) mats. *Eur Polym J*. 2005;41(3):423-432. doi:10.1016/j.eurpolymj.2004.10.027.

67.   Ballengee JB, Pintauro PN. Morphological Control of Electrospun Nafion Nanofiber

Mats. *J Electrochem Soc*. 2011;158(5):B568. doi:10.1149/1.3561645.

68.   Zhang J, Senger B, Vautier D, et al. Natural polyelectrolyte films based on layer-by layer deposition of collagen and hyaluronic acid. *Biomaterials*. 2005;26(16):3353-3361. doi:10.1016/j.biomaterials.2004.08.019.

69.   Angammana CJ, Jayaram SH. Investigation of the optimum electric field for a stable electrospinning process. *IEEE Trans Ind Appl*. 2012;48(2):808-815. doi:10.1109/TIA.2011.2180010.

70.   Scarlet R, Manea LR, Sandu I, Cramariuc B, Sandu AV. The Influence of the Needle - Collector Distance Upon the Characteristics of the Polyetherimide Nanofibres Obtained by Electrospinning. *Rev Chim*. 2012;63(8):777-782.

71.   Jarusuwannapoom T, Hongrojjanawiwat W, Jitjaicham S, et al. Effect of solvents on electro-spinnability of polystyrene solutions and morphological appearance of resulting electrospun polystyrene fibers. *Eur Polym J*. 2005;41(3):409-421. doi:10.1016/j.eurpolymj.2004.10.010.

72.   Chen HM, Yu DG. An elevated temperature electrospinning process for preparing acyclovir-loaded PAN ultrafine fibers. *J Mater Process Technol*. 2010;210(12):1551-1555. doi:10.1016/j.jmatprotec.2010.05.001.

73.   Liang T, Parhizkar M, Edirisinghe M, Mahalingam S. Effect of humidity on the generation and control of the morphology of honeycomb-like polymeric structures by electrospinning. *Eur Polym J*. 2014;61:72-82. doi:10.1016/j.eurpolymj.2014.09.020.

74.   Casper CL, Stephens JS. Controlling Surface Morphology of Electrospun Polysterene Fibers: Effect of Humidity and Molecular Weight in Electrospinning Process. *Macromolecules*. 2004;37:573-578.

75.   Supaphol P, Mit-Uppatham C, Nithitanakul M. Ultrafine electrospun polyamide-6 fibers: Effect of emitting electrode polarity on morphology and average fiber diameter. *J Polym Sci Part B Polym Phys*. 2005;43(24):3699-3712. doi:10.1002/polb.20671.

76.   Tang M, Ding S, Min X, et al. Collagen fi lms with stabilized liquid crystalline

phases and concerns on osteoblast behaviors. *Mater Sci Eng C*. 2016;58:977-985.

77.   Jha BS, Ayres CE, Bowman JR, et al. Electrospun Collagen: A Tissue Engineering Scaffold with Unique Functional Properties in a Wide Variety of Applications. *J Nanomater*. 2011;2011:1-15. doi:10.1155/2011/348268.

78.   Hohman MM, Shin M, Rutledge G, Brenner MP. Electrospinning and electrically forced jets. II. Applications. *Phys Fluids*. 2001;13(8):2221-2236. doi:10.1063/1.1384013.

79.   Carroll CP, Joo YL. Electrospinning of viscoelastic Boger fluids: Modeling and experiments. *Phys Fluids*. 2006;18(5). doi:10.1063/1.2200152.

80.   Fridrikh S V., Yu JH, Brenner MP, Rutledge GC. Controlling the Fiber Diameter during Electrospinning. *Phys Rev Lett*. 2003;90(14):144502. doi:10.1103/PhysRevLett.90.144502.

81.   Kirichenko, V.N., PETRYANOV, S.I., Suprun, N.N. and Shutov AA. Asymptotic radius of a slightly conducting liquid jet in an electric field. *Sov Phys Dokl*. 1986;31(January):611.

82.   Bhattacharjee PK, Schneider TM, Brenner MP, McKinley GH, Rutledge GC. On the measured current in electrospinning. *J Appl Phys*. 2010;107(4). doi:10.1063/1.3277018.

83.   Tang X-P, Si N, Xu L, Liu H-Y. Effect of flow rate on diameter of electrospun nanoporous fibers. *Therm Sci*. 2014;18(5):1447-1449. doi:10.2298/TSCI1405447T.

84.   Marcela L, Sánchez D, Rodriguez L, López M. Electrospinning : la era de las nanofibras. *Rev Iberoam polímeros*. 2014;14(1):10-27.

85.   Rafiei S, Maghsoodloo S, Noroozi B, Mottaghitalab V, Haghi AK. Mathematical modeling in electrospinning process of nanofibers : a detailed review. *Cellul chemestry Technol*. 2013;47:323-338.

86.   Rutledge GC, Warner SB. Electrostatic Spinning and Properties of Ultrafine Fibers. *Natl Text Cent Annu Rep*. 2002;M01-D22(November):1-10.

87.   Im JS, Jang J-SS, Lee Y-SS. Synthesis and characterization of mesoporous electrospun carbon fibers derived from silica template. *J Ind Eng Chem*. 2009;15(6):914-918. doi:10.1016/j.jiec.2009.09.024.

88.   Angammana CJ, Jayaram SH. A Theoretical Understanding of the Physi- cal Mechanisms of Electrospinning. *ESA Annu Meet Electrost*. 2011:1-9.

ANNEXES

1. Getting the fiber diameter by DiameterJ

You can obtain the average fiber diameters as follows:

1. Download and install ImageJ 1.48
2. Download DiameterJ plugin
3. Open ImageJ
4. Go to: "Plugins-->DiameterJ-- DiameterJ Segment SRM" to segment images.
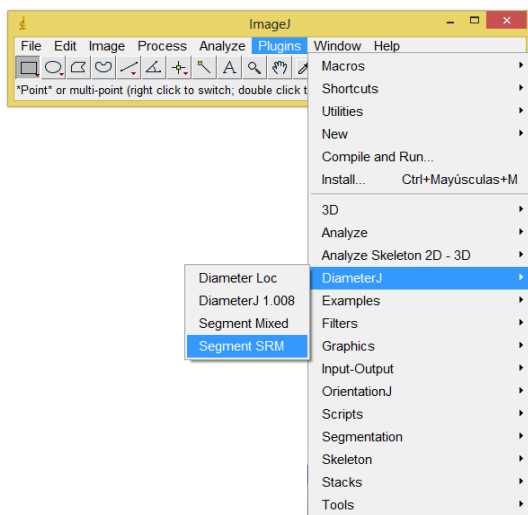
Figure 24. Image segmentation

5. A pop-up window will appear asking what folder you would like to analyze.
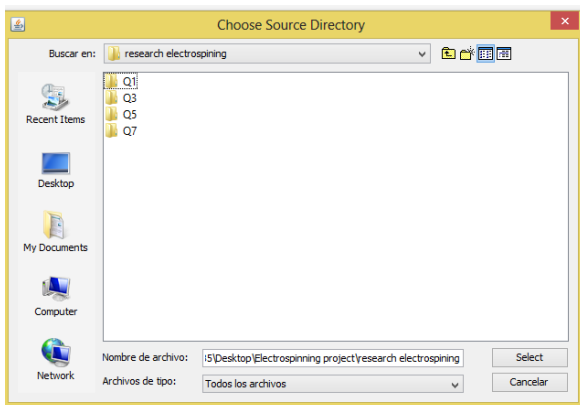
Figure 25. Choosing folder to analyze

6. A pop-up window will appear asking if you want to crop the image. If you want that software scan the entire image, you must write 2,

Figure 26. Option: crop the image

7. The code will produce three new folders within the folder where the images that you selected for analysis are located. One folder is called "Best Segmentation," another is called "Montage Images," and the third is called "Segmented Images.
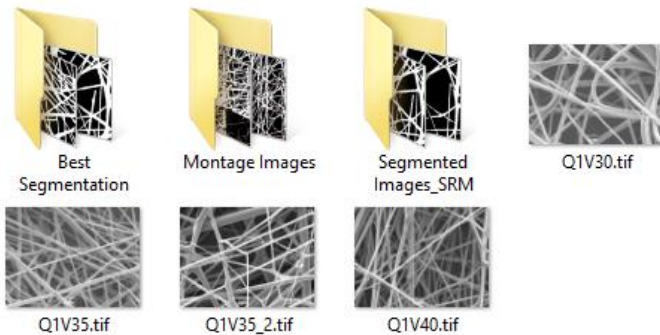
Figure 27. Yield of three new folders

The "Best Segmentation" folder contains no images. The "Montage Images" includes a montage comparison image of the original image with 8 different segmentation methodologies. Look at each of the montage images and find the name of the image with the most accurate representation of your fibers. Names of the images shown in the montage are on the bottom of each image in Red.
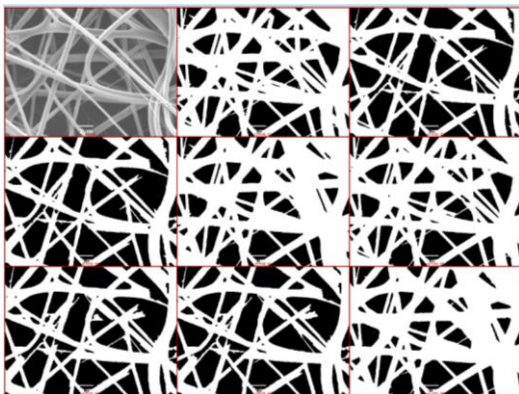
Figure 28. Choosing the best-segmented image

The "Segmented Images" folder has all of the segmented images from the montage images. Copy and paste the images you have determined to have the best segmentation into the "Best Segmentation" folder.

8. In ImageJ, go to:

"Plugins-->DiameterJ-->DiameterJ 1.008" to analyze the segmented image.
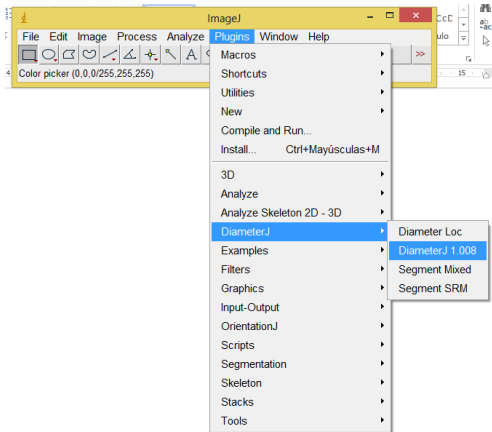
Figure 29. Opening Diameterj

9. A pop-up window will appear asking what folder you would like to analyze. You must choose "Best Segmentation" folder.
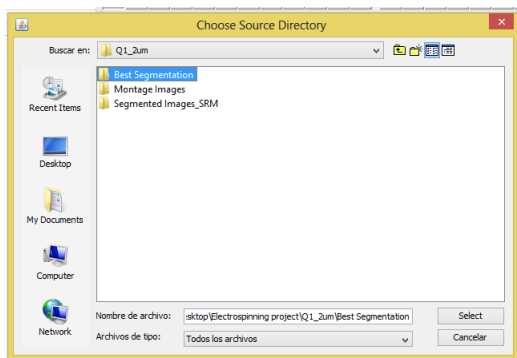
Figure 30. Choosing "the best segmentation" folder

Output files will be saved in the same location that the images the user selected are in DiameterJ will then analyze all images in the specified directory and will separate its analysis into three folders: "Diameter Analysis Images," "Histograms", and "Summaries." These folders will be located in the directory where the analyzed image is located.
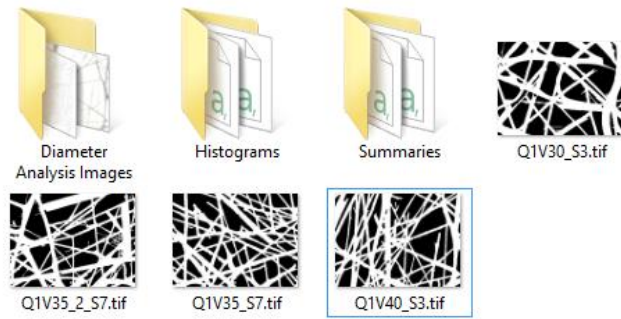
Figure 31. Diameter's output

The folder "Summaries" displays diameter values per each SEM image analyzed in pixels. I used a conversion factor of 0.112 pixels/nm when the scale bar was 2 µm and 0.0224 pixels/nm when this was 10 µm. I selected diameters from "histogram mean" because this measurement is more accurate for global averages of fiber diameter inasmuch as my images have not incredibly different fiber diameters.
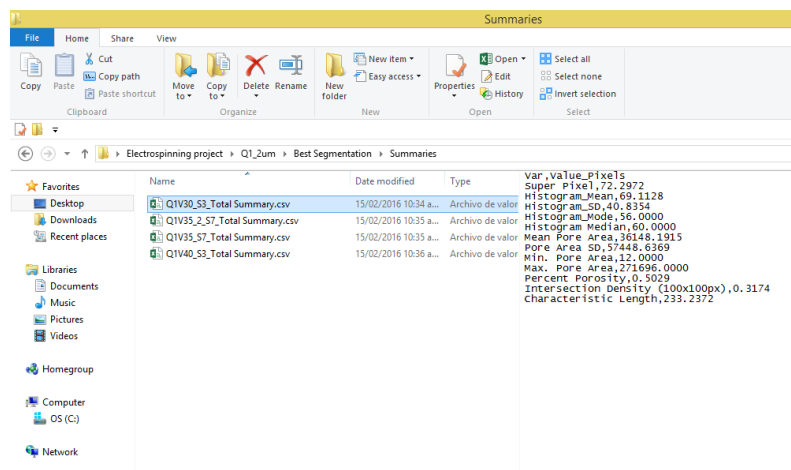
Figure 32 Results from summary folder

2. Results

Table 4. Diameter fiber (nm)

Voltage (kv)	Flow rate (mL/h)			
	1	3	5	7
30	273	408	840	511
	397	427	175	481
	296	242	367	598
Mean	322 ± 66	359 ± 102	460 ± 136	530 ± 61
35	438	413	587	316
	233	384	274	458
	461	451	385	383
Mean	378 ± 126	416 ± 33	415 ± 159	386 ± 71
40	442	336	396	366
	296	332	295	489
	310	365	440	522
Mean	349 ± 81	344 ± 18	377 ± 74	459 ± 82
45	227	321	358	378
	207	343	453	445
	227	394	313	308
Mean	220 ± 12	353 ± 37	375 ± 72	377 ± 68

3. Comparison between experimental data and theoretical calculations
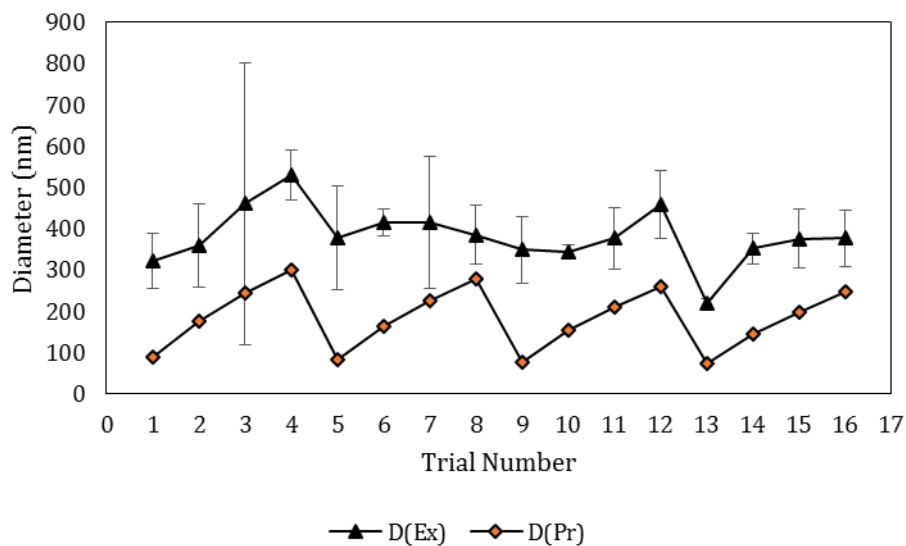
Figure 33. Comparison between experimental data and theoretical calculations